第 34 卷第 11 期
2018 年 11 月

无 机 化 学 学 报
CHINESE JOURNAL OF INORGANIC CHEMISTRY

Vol.34 No.11
2063-2072

卤素离子触发亚铁四面体笼的自旋状态转换

张海霞[1] 韩王康[1] 张峰丽[1] 何 威[1] 葛芳圆[1] 王娅琴[1] 晏晓东[1] 顾志国*,[1,2]

([1]江南大学化学与材料工程学院,合成胶体与生物技术教育部重点实验室,无锡 214122)

([2]江南大学化学与材料工程学院国际光响应分子与材料联合研究中心,无锡 214122)

摘要:合理构筑了 3 个具有固态自旋交叉特性的亚铁四面体笼状化合物 **1~3**。单晶 X 射线衍射分析证实了化合物是由 6 个咪唑席夫碱配体和 4 个亚铁离子组装形成的边导向封顶胶囊结构。金属中心占据四面体的顶点,而配体组成了四面体的边。这些笼状化合物的内部空腔被咪唑基团环绕,而外部则被取代苯环包围。一个阴离子客体被限域在笼状化合物空腔内,并与笼状化合物主体产生较强的相互作用。当在笼状化合物的乙腈溶液中加入卤素离子(Cl^-和 Br^-)时,溶液的颜色和 MLCT 峰强度会发生明显变化,表明亚铁四面体笼状化合物的自旋状态由低自旋向高自旋发生了转换。

关键词:金属有机笼;自旋交叉;卤素离子;主客体;自旋状态转换

中图分类号:O614.81+1 **文献标识码**:A **文章编号**:1001-4861(2018)11-2063-10

DOI:10.11862/CJIC.2018.233

Halide Triggered Spin State Switching of Iron(Ⅱ) Tetrahedral Cages

ZHANG Hai-Xia[1] HAN Wang-Kang[1] ZHANG Feng-Li[1] HE Wei[1]

GE Fang-Yuan[1] WANG Ya-Qin[1] YAN Xiao-Dong[1] GU Zhi-Guo*,[1,2]

([1]*Key Laboratory of Synthetic and Biological Colloids, Ministry of Education, School of Chemical and Material Engineering, Jiangnan University, Wuxi, Jiangsu* 214122, *China*)

([2]*International Joint Research Center for Photoresponsive Molecules and Materials, School of Chemical and Material Engineering, Jiangnan University, Wuxi, Jiangsu* 214122, *China*)

Abstract: Three iron(Ⅱ) tetrahedral cages **1~3** with solid state spin-crossover properties were rational constructed. Single crystal X-ray diffraction analysis confirmed the edge-capped capsule, which were assembled from six imidazole Schiff-base ligands and four iron(Ⅱ) ions. The metal centers occupy the vertices and each linker situates at the edges of the tetrahedron. The inner cavities of these cages are surrounded by imidazole groups, while the periphery is decorated by substituted phenyl rings. One of the counter anions is encapsulated at the central cavities and shows strong anion binding interactions with the cages. Interestingly, the iron(Ⅱ) cages in solution can change their spin states from low-spin (LS) to high-spin (HS) upon addition of halide, since tremendous change of solution color and absorption intensity of characteristic broad absorption MLCT bands when addition of halide (Cl^- and Br^-) to the CH_3CN solution of the cages. CCDC: 1560377, **1**; 1560378, **2**; 1560379, **3**.

Keywords: metal-organic cage; spin-crossover; halide; host-guest; spin state switching

收稿日期:2018-06-22。收修改稿日期:2018-07-18。

国家自然科学基金(No.21771089)、中央高校基本科研业务经费(No.JUSRP51725B,JUSRP51513)、江苏省双创团队项目和 MOE&SAFEA 111 项目(No.B13025)资助。

*通信联系人。E-mail:zhiguogu@jiangnan.edu.cn

0 Introduction

Crystalline spin-crossover (SCO) materials with tunable spin states under external perturbations such as temperature, light irradiation, pressure or magnetic field have been proved with attractive potential in display devices and data storage[1-2]. Compared with SCO in the solid state, the spin state switching in solution at room temperature can offer intriguing applications in solution-based chemosensing and switchable MRI contrast agents[3]. Nevertheless, for thermally induced spin transitions of molecules in solution, it often shows gradual and incomplete spin equilibrium due to the lack of cooperatively[4]. In the past few years, some effective approaches have been developed to achieve the spin state switching in solution: (1) light induced *cis-trans* configuration transition of ligands and/or coordination number change to turn the ligand field strength and spin state of metal complexes[5]; (2) redox process at a redox-active ligand to control spin state of metal centre in solution[6]; (3) the special designed noncovalent interactions, such as hydrogen bonding and anion binding, have emerged as powerful tools to affect the spin state of SCO complexes in solution[7].

For the research of anion binding and its influence on spin state of metal centres in solution, metal-organic cages with plentiful positive charges and intrinsic cavities may provide a unique platform. Since metal-organic cages have shown great affinity and selectivity in guest binding, the inner cavities of cages enable to establish abundant intermolecular interactions with the encapsulated guests[8].

Recently, solution SCO behaviours of supramolecular iron(Ⅱ) cubic and tetrahedral cages have been proved to be slightly affected by small molecules guest encapsulation[9].

However, to the best of our knowledge, the examples about encapsulated anionic guests in metal-organic cages to influence the SCO properties in solution are still scare[9b], and the realization of sensitive spin state change based on metal-organic cages from low-spin (LS) to high-spin (HS) in solution at room temperature is still a challenge.

To develop anion dependent SCO cages, three main factors must be considered: (1) it is crucial to choose the assembly ligand with appropriate ligand field strength to insure metal centres undergoing SCO behaviour; (2) the cavity shape and volume of the rational designed cages should be suitable for capturing anionic guests; (3) the appending of hydrogen-bonding or other anion-binding groups inside the cage cavities would create chelating pockets capable of selective interaction with anions. With these in mind, three new iron(Ⅱ) tetrahedral cages with imidazole-imine (C=N) type ligands, which have appropriate ligand field strength to allow SCO for Fe(Ⅱ) centre, were prepared and characterized. Their solid state magnetic properties and halide triggered spin state switching in solution are demonstrated (Scheme 1).

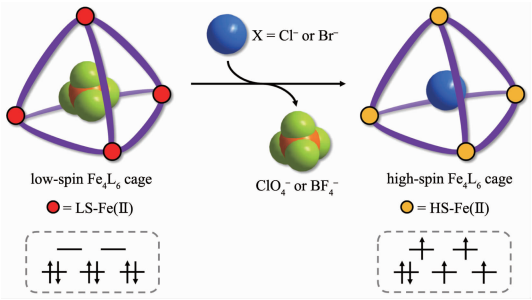

Scheme 1 Schematic representation of the halide triggered spin state switching of iron(Ⅱ) tetrahedral cages

1 Experimental

1.1 Chemical materials and physical measurements

All reagents and solvents were reagent grade, purchased from commercial sources and used without further purification.

Caution: Although no problems were encountered in this work, the perchlorate salt was potentially explosive. Thus, this starting material should be handled in small quantities and with great caution!

Infrared spectra were measured with a Nicolet 6700 FT-IR spectrophotometer with ATR attachment in the range of 500~4 000 cm^{-1} region. ^1H NMR spectra were recorded on AVANCE Ⅲ (400 MHz) instrument at 298 K using standard Varian or Bruker software,

and chemical shifts were reported downfield from tetramethylsilane. Element analyses were conducted on elementar corporation vario EL Ⅲ analyzer. UV-Vis absorbance spectra were collected on Shimadzu UV-2101 PC scanning spectrophotometer. Variable-temperature magnetic susceptibilities on crystalline samples were performed on a Quantum Design MPMS-XL-7 SQUID magnetometer with an applied magnetic field of 1 kOe over the temperature range of 2~400 K. The molar susceptibility was corrected for diamagnetic contributions using Pascal′s constants and the increment method. Samples were restrained with petroleum jelly to prevent decomposing of the crystallites. Thermal gravimetric analysis (TGA) was carried out on a Waters TGA Q500 by heating the samples from 40 to 600 ℃ under nitrogen atmosphere at a heating rate of 15 ℃·min^{-1}.

1.2 Preparation of the complexes

1.2.1 Synthesis of 1,2-di(imidazole-2-carboxaldehyde) ethane

The 1,2-di(imidazole-2-carboxaldehyde)ethane were synthesized according to the previously reported procedures with slightly modifications[10]. All experimental details regarding the synthesis and the characterization of the compounds were presented in the supporting information.

1.2.2 Synthesis of cages **1~3**

Cage **1**: 1,2-di(imidazole-2-carboxaldehyde)ethane (43.6 mg, 0.2 mmol), (*R*)-1-phenylethylamine (48.9 mg, 0.4 mmol) and $Fe(BF_4)_2·6H_2O$ (45.0 mg, 0.13 mmol) were added to a flask with 20 mL of acetonitrile in nitrogen atmosphere. The solution was stirred and heated at 80 ℃ for 2 h, cooled to room temperature. Then, the resulting purple solution was filtered. Cage **1** was precipitated as dark purple crystals through slow diffusion of diethyl ether into the filtrate at room temperature. Yield: 61%. Anal. Calcd. for $C_{156}H_{168}B_8F_{32}Fe_4N_{36}$(%): C, 54.07; H, 4.88; N, 14.55; Found(%): C, 54.51; H, 4.61; N, 14.74. IR (cm^{-1}): 3 132, 3 030, 2 981, 1 614, 1 571, 1 531, 1 484, 1 441, 1 387, 1 364, 1 304, 1 054, 918, 838, 762, 706, 625.

Cage **2**: 1,2-di(imidazole-2-carboxaldehyde)ethane (43.6 mg, 0.2 mmol), (*S*)-1-(4-chlorophenyl)ethylamine (62.3 mg, 0.4 mmol) and $Fe(ClO_4)_2·6H_2O$ (48.4 mg, 0.13 mmol) were added to a flask with 20 mL of acetonitrile in nitrogen atmosphere. The solution was stirred and heated at 80 ℃ for 2 h, cooled to room temperature. Then, the resulting purple solution was filtered. Cage **2** was precipitated as dark purple crystals through slow diffusion of diethyl ether into the filtrate at room temperature. Yield: 48%. Anal. Calcd. for $C_{156}H_{156}Cl_{20}Fe_4N_{36}O_{32}$(%): C, 47.08; H, 3.95; N, 12.67; Found(%): C, 47.39; H, 4.41; N, 12.86. IR (cm^{-1}): 3 134, 3 030, 2 978, 1 616, 1 566, 1 530, 1 489, 1 440, 1 385, 1 305, 1 073, 1 010, 970, 917, 831, 771, 711, 687, 619.

Cage **3**: the preparation was similar to that described for cage **2** except that (*S*)-1-(4-bromophenyl) ethylamine (80.0 mg, 0.4 mmol) instead of (*S*)-1-(4-chlorophenyl)ethylamine was used. Dark purple crystals of cage **3** were obtained. Yield: 54%. Anal. Calcd. for $C_{156}H_{156}Br_{12}Cl_8Fe_4N_{36}O_{32}$(%): C, 41.52; H, 3.48; N, 11.17; Found(%): C, 41.88; H, 3.90; N, 11.04. IR (cm^{-1}): 3 134, 2 978, 1 622, 1 566, 1 526, 1 485, 1 434, 1 384, 1 300, 1 072, 1 008, 967, 914, 823, 759, 708, 688, 618.

1.3 General procedure for halide titrations experiments

Stock solutions of the cage complexes were made up in acetonitrile with the concentrations being 63 μmol·L^{-1}. And the stock solutions of the anionic guest were also made up in the acetonitrile with the concentrations being 0.05 mol·L^{-1} to avoid the dilution effects. The UV-Visible spectra data for the additions of the anionic guest solution using 10 μL syringe to a 3 mL of the cage complex solution (1.0 cm path length for the cuvette) were collected. The solutions were mixed by repeated inversion, and the absorption spectra were recorded after mixing for 1 min.

1.4 General procedure for Ag(Ⅰ) back-titrations experiments

Firstly, 50 μL tetrabutylammonium salts (0.05 mol·L^{-1}, CH_3CN) were added to 3 mL solution of cage complex (63 μmol·L^{-1}, CH_3CN). Waiting for one minute, a solution of $AgBF_4$ or $AgClO_4$ (0.05 mol·L^{-1}) was added step by step using 10 μL syringe, and the

UV-Visible absorption spectra were recorded after mixing for 1 min.

1.5 X-ray diffraction studies details

The crystal structures were determined on a Siemens (Bruker) SMART CCD diffractometer using monochromated Mo $K\alpha$ radiation (λ=0.071 073 nm). Cell parameters were retrieved using SMART software and refined using SAINT[11] on all observed reflections. The highly redundant data sets were reduced using SAINT and corrected for Lorentz and polarization effects. Absorption corrections were applied using SADABS[12] supplied by Bruker. Structures were solved by direct methods using the program SHELXL-97[13]. All of the non-hydrogen atoms except the anions were refined with anisotropic thermal displacement coefficients. Hydrogen atoms of organic ligands were located geometrically and refined in a riding model, whereas those of solvent molecules were not treated during the structural refinements. Disorder was modelled using standard crystallographic methods including constraints, restraints and rigid bodies where necessary. For cage **1**, two tetrafluoroborate anions (the fluorine atom F(1B), F(2B), F(3B) and F(4B) bound to B(1B), the fluorine atom F(1F), F(2F), F(3F) and F(4F) bound to B(1F)) are disordered. For cage **2**, despite rapid handling and long exposure times, the data collected are less than ideal quality, and one perchlorate anion no reasonable could be found. For cage **3**, two 1-(4-bromophenyl)ethylamine group (C(33)~C(40) and Br(3)) are disorder, and the oxygen atoms bound to Cl(5) are disordered. The crystals of cages **1**~**3** decayed rapidly out of solvent. Nevertheless, the data for cages **1**~**3** are of more than sufficient quality to unambiguously establish the connectivity of the structures. Reflecting the instability of the crystals, there is a large area of smeared electron density present in the lattice. Despite many attempts to model this region of disorder as a combination of solvent molecules no reasonable fit could be found and accordingly this region was treated with the SQUEEZE[14] function of PLATON[15]. Final crystallographic data for cages **1**~**3** are listed in Table 1, and the selected bond lengths (nm) and angles (°) are listed in Table S1 (Supporting Information) and anion binding interactions (nm) between the imidazole C-H groups and the encapsulated anion for cages **1**~**3** in Table S2.

CCDC: 1560377, cage **1**; 1560378, cage **2**; 1560379, cage **3**.

Table 1 Crystallographic data for cages 1~3

	cage **1**	cage **2**	cage **3**
Formula	$C_{156}H_{168}B_8F_{32}Fe_4N_{36}$	$C_{160}H_{164}Cl_{18}Fe_4N_{38}O_{24}$	$C_{156}H_{156}Br_{12}Cl_8Fe_4N_{36}O_{33.26}$
Formula weight	3 465.14	3 864.79	4 533.29
T / K	173(2)	173(2)	173(2)
Crystal system	Triclinic	Orthorhombic	Orthorhombic
Space group	$P\bar{1}$	$C222_1$	$C222_1$
a / nm	1.830 33(19)	2.005 18(11)	2.015 94(13)
b / nm	1.877 5(2)	3.333 03(15)	3.347 33(17)
c / nm	1.897 6(2)	3.434 6(2)	3.435 8(2)
α / (°)	62.228(3)		
β / (°)	63.553(3)		
γ / (°)	77.863(3)		
V / nm^3	5.1661(10)	22.954(2)	23.185(2)
Z	1	4	4
D_c / (Mg·m^{-3})	1.114	1.118	1.229
μ / mm^{-1}	0.354	0.516	2.468
F(000)	1 788	7 968	9 080
θ range / (°)	1.23~22.50	3.02~24.25	2.95~25.00

Continued Table 1

Index ranges	$-19 \leqslant h \leqslant 19$, $-19 \leqslant k \leqslant 20$, $-20 \leqslant l \leqslant 20$	$-23 \leqslant h \leqslant 23$, $-38 \leqslant k \leqslant 37$, $-35 \leqslant l \leqslant 39$	$-23 \leqslant h \leqslant 23$, $-37 \leqslant k \leqslant 36$, $-40 \leqslant l \leqslant 39$
Reflection collected	29 723	50 325	54 201
GOF (F^2)	1.039	1.064	1.106
R_1[a], wR_2[b] [$I>2\sigma(I)$]	0.096 3, 0.228 1	0.080 4, 0.202 8	0.065 9, 0.150 1
R_1[a], wR_2[b] (all data)	0.172 3, 0.258 5	0.115 8, 0.224 0	0.117 0, 0.166 8

[a] $R_1=\sum||F_o|-|F_c||/\sum|F_o|$; [b] $wR_2=[\sum w(F_o^2-F_c^2)^2/\sum w(F_o^2)]^{1/2}$.

2　Results and discussion

2.1　Preparation and characterization of cages 1~3

The three tetrahedral cages $[Fe_4(L_1)_6](BF_4)_8$ (**1**) (L_1=1,2-di((imidazol-2-ylmethylene)-(*R*)-1-phenylethanamine)ethane), $[Fe4(L_2)_6](ClO_4)_8$ (**2**) (L_2=1,2-di((imidazol-2-ylmethylene)-(*S*)-1-(4-chlorophenyl)ethylamine)ethane) and $[Fe_4(L_3)_6](ClO_4)_8$ (**3**) (L_3=1,2-di((imidazol-2-ylmethylene)-(*S*)-1-(4-bromopheny)ethylamine)ethane) were obtained by the self-assembly reactions of flexible 1,2-di(imidazole-2-carboxaldehyde)ethane, iron(Ⅱ) ions and amine components in a 3∶2∶6 molar ratio in acetonitrile solution. IR spectra of cages **1**~**3** show strong absorptions in the region around 1 570~1 616 cm^{-1}, which are typical for stretching of imidazole-imine (C=N) groups. The peaks at about 1 073 or 1 051 cm^{-1} reveal the existence of ClO_4^- or BF_4^- (Fig.S3~S5). The TGA analyses showed that solvent molecules existed in the cage **1**~**3** (Fig.S6).

Single crystal X-ray diffraction confirmed the edge-capped tetrahedral capsule structures for **1**~**3** (Fig.1). The iron(Ⅱ) centre coordinated to six nitrogen atoms from three different ligands forms a distorted octahedral FeN_6 geometry, and the four six-coordinated octahedral Fe(Ⅱ) metal nodes are bridged by six C_2-symmetric ligand linkers forming a tetrahedral cage. The metal centres occupies the vertices and the linker situates at the edges of the tetrahedron. The average Fe-N bond lengths of cages **1**~**3** range from 0.189 2 to 0.199 2 nm, which are typical for low-spin state Fe(Ⅱ) centre[16]. In each $[Fe_4L_6]^{8+}$ cation, twelve intramolecular face-to-face π-π stacking interactions are generated between each parallel phenyl ring and imidazole ring of the adjacent ligand, which further stabilize the supramolecular structures (Fig.S7). The average center-center distances of π-π interactions for cages **1**~**3** range from 0.382 1 to 0.384 7 nm. The average Fe⋯Fe separations along the edges lie in the range from 0.903 9 to 0.904 9 nm for cages **1**~**3**.

Furthermore, it is worth noting that one of the ClO_4^- or BF_4^- anions is encapsulated at the central cavity, and the remaining anions are decorated around the periphery of cages **1**~**3**. The encapsulated anion shows strong anion binding interactions with the cages (Fig.2a). Each terminal F atoms (or O atoms) of the

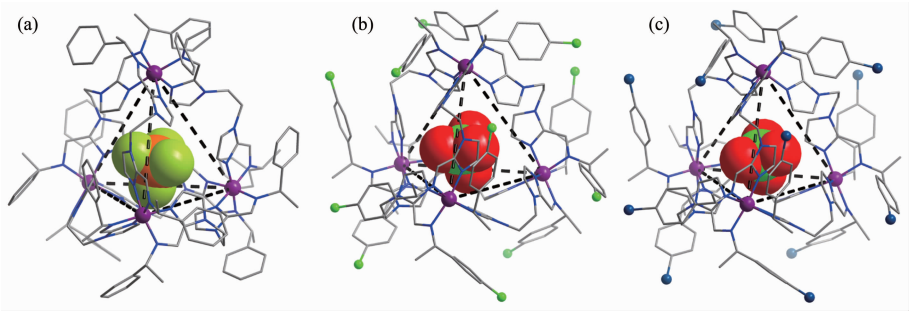

C: grey; N: blue; Fe: purple; B: orange; F: lime; Cl: bright green; O: red; Br: dark teal; All H atoms, solvent molecules and the remaining anions have been removed for clarity

Fig.1　X-ray crystal structures of iron(Ⅱ) tetrahedral cages **1** (a), **2** (b) and **3** (c) showing one encapsulated anion in space-filling mode

encapsulated tetrafluoroborate anion or perchlorate anion binds with three C-H protons of imidazole moieties at each tetrahedral vertex in the internal surface of the cage (Fig.2b), while each C_2-symmetric ligand binds the encapsulated anion through two C–H⋯F or C–H⋯O interactions (Fig.2c). The average anion binding of H⋯F or H⋯O distances for cages **1~3** range from 0.250 3 to 0.261 2 nm (Table S3). In addition, around the periphery, each tetrahedral vertex of cages decorated one anion through C–H⋯F or C–H⋯O binding between the terminal F atoms (or O atoms) of anions and the C-H protons of imidazole-imine groups (Fig.S8). The space-filling pictures derived from the crystallographic data show that there is a gap in the centre of the triangular faces and the encapsulated anion is clearly visible through the window in the centre of each face (Fig.S9 ~S10). Additionally, in the solid state the bridging ligands are substantially folded, and a more relaxed conformation in solution would result in larger windows[17], such that each face of the cage possesses a large enough window for the anion to diffuse into and out of the cavity.

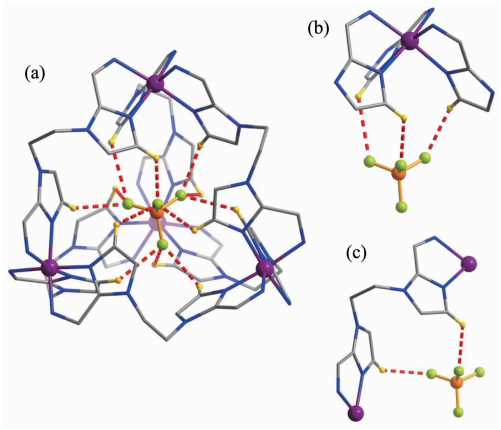

All H atoms, solvent molecules, the remaining anions and the twelve substituted phenyl ring group around the periphery of four vertices have been removed for clarity

Fig.2 (a) Anion binding between the encapsulated anion and the C-H protons of imidazole moieties for cages **1~3**; (b) Close-up view of one anion binding with three C-H protons of each vertex of the cages; (c) Close-up view of one anion binding with two C-H protons of each side of the cages

2.2 Magnetic properties

The temperature dependent magnetic susceptibilities data on polycrystalline samples of cages **1~3** were collected in the cooling mode from 400 to 2 K. As shown in the Fig.3, gradual and incomplete spin-crossover behaviours for cages **1~3** were observed. For cage **1**, the $\chi_M T$ value is 10.35 $cm^3 \cdot K \cdot mol^{-1}$ at 400 K (Fig.3a), which is lower than the expected value for four S=2 high spin Fe(Ⅱ) ions. Then, the $\chi_M T$ values gradually decreases to 0.75 $cm^3 \cdot K \cdot mol^{-1}$ at 200 K and almost constant at the low temperature, which suggests that the Fe(Ⅱ) centers are in the LS state below 200 K. For cages **2** and **3**, the $\chi_M T$ values are 8.80 and 8.81 $cm^3 \cdot K \cdot mol^{-1}$ at 400 K, respectively (Fig.3b~3c). Upon cooling from 200 to 20 K, the $\chi_M T$ value remains almost constant (proximity to 4.81 $cm^3 \cdot K \cdot mol^{-1}$ for cage **2** and 6.23 $cm^3 \cdot K \cdot mol^{-1}$ for cage **3**). The change of $\chi_M T$ values below 20 K are probably

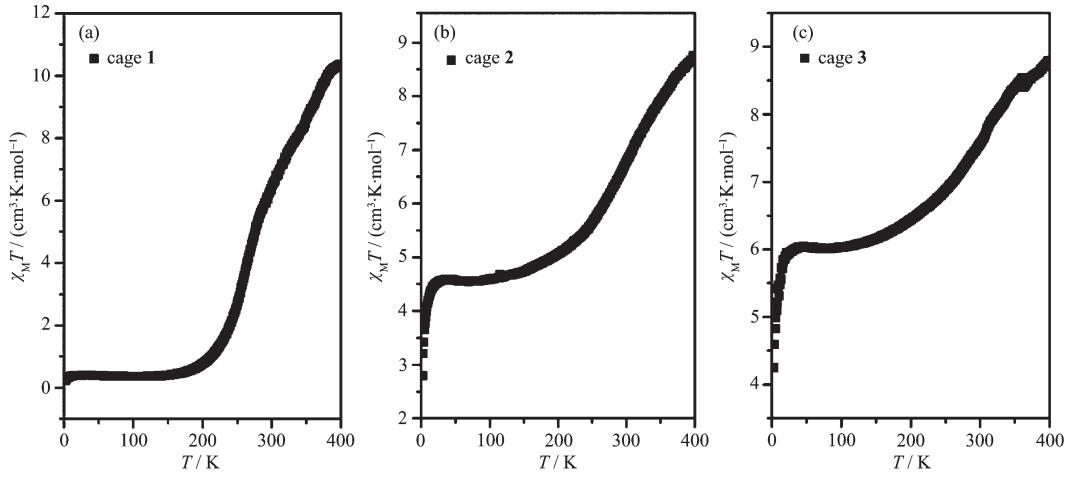

Fig.3 Variable-temperature solid-state magnetic susceptibility for cages **1** (a), **2** (b) and **3** (c)

due to the antiferromagnetic coupling of the object ions[18].

2.3 Spin state switching experiments

Based on the detailed structural analysis, the three iron(Ⅱ) tetrahedral cages **1**~**3** possess multiple cationic charge, and the intrinsic cavities show abundant C–H⋯F or C–H⋯O binding interactions with the encapsulated anion for the stabilization of low-spin cages. These features provide a unique platform to influence the spin transition properties through anion binding in solution. The UV-Vis spectra of cages **1**~**3** in acetonitrile solution all exhibit metal-to-ligand charge transfer (MLCT) processes with characteristic broad bands around 536 nm, which confirms the low-spin state of **1**~**3** in solution at room temperature (Fig.S11~S13). Since the low-spin iron(Ⅱ) is expected to feature more intense MLCT transitions, the spin state change in principle could be followed by monitoring the absorption changes of the MLCT through UV-Vis spectra.

The thermally induced spin transitions of cages **1**~**3** in solution were investigated by variable temperature UV-Vis spectra. It gives rise to a decrease in the intensity of the characteristic MLCT absorption band in UV-Vis spectra as the temperature warms from 20 to 80 ℃ (Fig.S14~S16), indicating that the iron(Ⅱ) center in **1**~**3** change from the low-spin state to high-spin state. However, the thermally induced spin transitions of cages **1**~**3** in solution are gradual, and the temperature range is wide. In order to develop a more effective approach to tune the spin state of cages **1**~**3** in solution, a series of anion titrations experiments were carried out. And it was found that the addition of halide (Cl^- and Br^-) had major influence on the spin state of cages **1**~**3**.

The solution color of cages **1**~**3** dramatically changed from violet red to pale yellow with titration of TBACl in acetonitrile, which was easily monitored by the naked eye, suggesting that the spin state transition in solution (Fig.4). Additionally, tremendous spectral changes in the UV-Vis spectra were observed. The absorption intensity of characteristic broad absorption MLCT bands at about 536 nm significantly decreased for cages **1**~**3** after the step by step addition of Cl^- (Fig.5a, 5c and 5e). Binding isotherms showed that the absorption intensity at 490, 506, 536 and 566 nm undergo a rapid decline with the addition of Cl^-, and then reach a platform (Fig.5b, 5d and 5f). These results demonstrate that the sensitive and significant change with spin state from low-spin to high-spin of the metal center for iron(Ⅱ) cages **1**~**3** in solution upon addition of Cl^-. Similar color change and UV-Vis monitored results were also observed when titrations of cages **1**~**3** with TBABr (Fig.S17~S19). Ag(Ⅰ) back-titration experiments were carried out. The addition of $AgBF_4$ or $AgClO_4$ to the HS pale yellow solution led to a reproduction of LS red solution (Fig.S20), and the absorption intensity of MLCT bands was observed to gradually increase (Fig.S21 ~S23). However, the absorption intensity of MLCT bands in UV-Vis spectra showed a slight increase (Fig.S24) when titrations of cages **1**~**3** with TBAI.

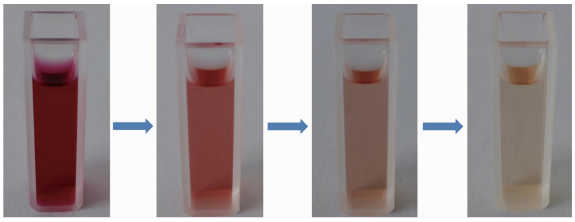

Fig.4 Photographs of cage **1** in CH_3CN solutions upon addition of tetrabutylammonium salts of Cl^-

In order to gain further insight into the halide trigged spin state switching behaviors of cages **1**~**3**, the ^1H NMR titration experiments were tried. Unfortunately, this experiment was infeasible due to the significant precipitation occurred upon addition of TBACl or TBABr at the concentration of cages **1**~**3** (65 mmol·L^{-1}) used for ^1H NMR measurements. Even so, the precipitates were collected, and the variable-temperature magnetic susceptibility measurements of the corresponding precipitates showed that they were all in high spin state (Fig.S25). These results further confirmed that cages **1**~**3** with halide anions (Cl^- and Br^-) in solid state were in high spin state.

From the single crystal X-ray diffraction analysis of cages **1**~**3**, efficient anion-cage interactions are formed through C–H⋯F or C–H⋯O interactions

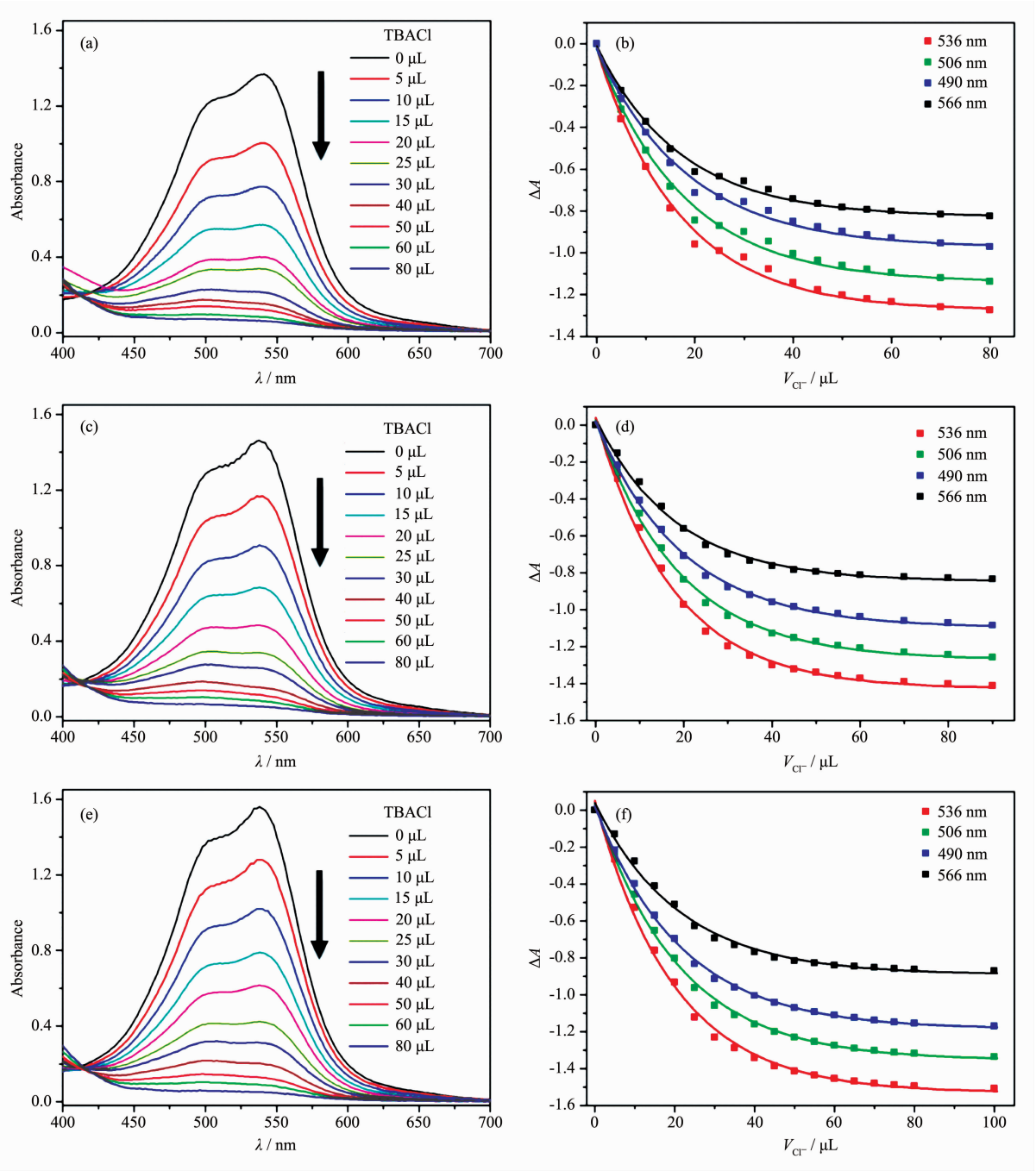

$c_{complex}$=63 μmol·L^{-1}, $V_{complex}$=3 mL; c_{TBACl}=0.05 mol·L^{-1}

Fig.5 Plot of the absorption changes for cages **1** (a), **2** (c) and **3** (e), and binding isotherms with fitted curves for cages **1** (b), **2** (d) and **3** (f) titrated with tetrabutylammonium salts of Cl in a CH_3CN solution

between the encapsulated BF_4^- or ClO_4^- anion and the ligands. These interactions can increase the σ-donating ability of the ligands bound to Fe(Ⅱ) ions, which thus contributes to stabilization of the low-spin state[19]. For titrations of cages **1**~**3** with halide in solution, we speculate that the halide anions displace the inner and peripheral BF_4^- or ClO_4^- anions due to the diffusional exchange and strong electrostatic interaction between the halide and cage host. However, the small volume of Cl^- (0.019 51 nm^3) and Br^- (0.025 52 nm^3) could not match well with the cavity size of cages **1**~**3**[20], so they will not be able to interact with the cage superstructure effectively and the anion binding interactions are weakened even disappeared, which

causes the LS to HS spin state transition for cages **1**~**3**. Since the volume of I^- (0.036 62 nm^3) gets much larger than Cl^- and Br^-, the effective anion-π interactions may existence between the encapsulated I^- and the twelve imidazole groups in the internal surface of the cages[21], which results to a slight more stabilization of the low-spin state for iron(Ⅱ) centers than BF_4^- or ClO_4^- anions. Therefore, it is implying that the anion binding interactions inside the cage cavity and around the periphery may play an important role in realizing the spin state transition in solution for cages **1**~**3**.

3 Conclusions

In summary, three SCO active tetrahedral iron(Ⅱ) cages were prepared and exhibited sensitive halide (Cl^- or Br^-) triggered spin state change from low-spin to high-spin in solution. Anionic guests induced spin state switching based on the host-guest chemistry in metal-organic cage opens new avenues for tuning the spin-crossover properties in solution at room temperature.

Supporting information is available at http://www.wjhxxb.cn

References:

[1] (a)Halcrow M A. *Chem. Soc. Rev.*, **2011**,**40**:4119-4142
(b)Bousseksou A, Molnar G, Salmon L, et al. *Chem. Soc. Rev.*, **2011**,**40**:3313-3335
(c)Cook Kershaw L J, Mohammed R, Sherborne G, et al. *Coord. Chem. Rev.*, **2015**,**289**:2-12
(d)Tao J, Wei R J, Huang R B, et al. *Chem. Soc. Rev.*, **2012**, **41**:703-737
(e)Manrique-Juárez M D, Mathieu F, Laborde A, et al. *Adv. Funct. Mater.*, **2018**:1801970
(f)WANG Yu-Xia(王玉侠), QIU Dan(邱丹), XI Sai-Fei(奚赛飞), et al. *Chinese J. Inorg. Chem.*(无机化学学报), **2016**, **32**(11):1965-1972

[2] (a)Khusniyarov M M. *Chem. Eur. J.*, **2016**,**22**:15178-15191
(b)Guionneau P. *Dalton. Trans.*, **2014**,**43**:382-393
(c)Kahn O, Martinez C J. *Science*, **1998**,**279**:44-48
(d)Rosner B, Milek M, Witt A, et al. *Angew. Chem. Int. Ed.*, **2015**,**54**:12976-12980
(e)Zenere K A, Duyker S G, Trzop E, et al. *Chem. Sci.*, **2018**, **9**(25):5623-5629

[3] (a)Samanta S, Demesko S, Dechert S, et al. *Angew. Chem. Int. Ed.*, **2015**,**54**:583-587
(b)Dommaschk M, Schutt C, Venkataramani S, et al. *Dalton. Trans.*, **2014**,**43**:17395-17405

[4] (a)Shores M P, Klug C M, Fiedler S R. *Spin-Crossover Materials*: *Properties and Applications*. Halcrow M A Ed., Oxford: Wiley-Blackwell, **2013**:281-301
(b)Weber B, Walker F A. *Inorg. Chem.*, **2007**,**46**:6794-6803

[5] (a)Hasegawa Y, Kume S, Nishihara H. *Dalton. Trans.*, **2009**,**2**:280-284
(b)Heitmann G, Schütt C, Herges R. *Eur. J .Org. Chem.*, **2016**,**22**:3817-3823
(c)Venkataramani S, Jana U, Dommaschk M, et al. *Science*, **2011**,**331**:445-448
(d)Thies S, Sell H, Schütt C, et al. *J. Am. Chem. Soc.*, **2011**,**133**:16243-16250

[6] (a)Schmitz M, Seibel M, Kelm H, et al. *Angew. Chem. Int. Ed.*, **2014**,**53**:5988-5992
(b)Wilson R K, Brooker S. *Dalton. Trans.*, **2013**,**42**:12075-12078
(c)Miller J S, Min K S. *Angew. Chem. Int. Ed.*, **2009**,**48**: 262-272

[7] (a)Young M C, Liew E, Ashby J, et al. *Chem. Commun.*, **2013**, **49**:6331-6333
(b)Ono K, Yoshizawa M, Akita M, et al. *J. Am. Chem. Soc.*, **2009**,**131**:2782-2783
(c)Ni Z, Shores M P. *J. Am. Chem. Soc.*, **2009**,**131**:32-33
(d)Ni Z, McDaniel A M, Shores M P. *Chem. Sci.*, **2010**,**1**:615-621
(e)Ni Z, Shores M P. *Inorg. Chem.*, **2010**,**49**:10727-10735

[8] (a)Rissanen K. *Chem. Soc. Rev.*, **2017**,**46**:2638-2648
(b)Zarra S, Wood D M, Roberts D A, et al. *Chem. Soc. Rev*, **2015**,**44**:419-432
(c)Ahmad N, Younus HA, Chughtai A H, et al. *Chem. Soc. Rev.*, **2015**,**44**:9-25
(d)Ramsay W J, Ronson T K, Clegg J K, et al. *Angew. Chem. Int. Ed.*, **2013**,**52**:13439-13443
(e)Ward M D, Hunter C A, Williams N H. *Chem. Lett.*, **2017**, **46**:2-9
(f)Metherell A J, Cullen W, Williams N H, et al. *Chem. Eur. J.*, **2018**,**24**:1554-1560

[9] (a)Struch N, Bannwarth C, Ronson T K, et al. *Angew. Chem. Int. Ed.*, **2017**,**56**:4930-4935
(b)Bilbeisi R A, Zarra S, Feltham H L, et al. *Chem. Eur. J.*, **2013**,**19**:8058-8062

[10](a)Ren D H, Qiu D, Pang C Y, et al. *Chem. Commun.*, **2015**, **51**:788-791
(b)Zhang F L, Chen Q J, Qin L F, et al. *Chem. Commun.*, **2016**,**52**:4796-4799

[11]*SAINT-Plus, Version* 6.02, Bruker Analytical X-ray System, Madison, WI, **1999**.

[12]Sheldrick G M. *SADABS*, Bruker Analytical X-ray Systems, Madison, WI, **1996**.

[13]Sheldrick G M. *SHELXTL*-97, University of Göttingen, Göttingen, Germany, **1997**.

[14]van der Sluis P, Spek A L. *Acta Crystallogr. Sect. A*: *Found. Crystallogr.*, **1990**,**A46**:194-201

[15]Spek A L. *Acta Crystallogr. Sect. D*: *Biol. Crystallogr.*, **2009**, **D65**:148-155

[16]Brooker S. *Chem. Soc. Rev.*, **2015**,**44**:2880-2892

[17]Paul R L, Argent S P, Jeffery J C, et al. *Dalton. Trans.*, **2004**,**21**:3453-3458

[18](a)Vostrikova K E, Luneau D, Wemsdorfer W, et al. *J. Am. Chem. Soc.*, **2000**,**122**:718-719

(b)Liu Y C, Hua S A, Cheng M C, et al. *Chem. Eur. J.*, DOI: 10.1002/chem.201801325

[19](a)Luo Y H, Nihei M, Wen G J, et al. *Inorg. Chem.*, **2016**,**55**: 8147-8152

(b)Nemec I, Herchel R, Travnicek Z. *Dalton. Trans.*, **2015**, **44**:4474-4484

[20]Darawsheh M, Barrios L A, Roubeau O, et al. *Chem. Eur. J.*, **2016**,**22**:8635-8645

[21]Mooibroek T J, Gamez P. *CrystEngComm*, **2013**,**15**:1802-1805